Cooling system of STRATOFLY hypersonic vehicle: conceptual design, numerical analysis and verification

33RD CONGRESS
OF THE INTERNATIONAL COUNCIL
OF THE AERONAUTICAL SCIENCES
STOCKHOLM, SWEDEN, 4-9 SEPTEMBER, 2022

ICAS 2022 SWEDEN

COOLING SYSTEM OF STRATOFLY HYPERSONIC VEHICLE: CONCEPTUAL DESIGN, NUMERICAL ANALYSIS AND VERIFICATION

Roberto Scigliano[1], Valeria De Simone[1], Roberta Fusaro[2], Davide Ferretto[2] , Marco Marini[1], Nicole Viola[2]

[1]Italian Aerospace Research Centre (CIRA), Capua Italy, r.scigliano@cira.it
[2]Politecnico di Torino (PoliTo), Torino Italy

Abstract

This paper describes the thermal design processes of STRATOFLY hypersonic vehicle cooling system showing either the methodology and the supporting FEM numerical simulations. It focuses on two different regions that are both subjected to severe overheating: air-intake leading edges and the combustion chamber. Final remarks on structure survivability are presented.

Keywords: Hypersonic, Aerothermodynamics, FEM, TPS, heat pipe

1. Introduction

Commercial hypersonic transport represents one of the main goals of next future economic and technological challenges. Designing a civil high-speed aircraft for passenger transportation means evaluating technical, environmental and economic viability in combination with human factors, social acceptance, implementation and operational aspects.

In the past years, some innovative high-speed aircraft configurations have been proposed and in-depth evaluated with the main goal of demonstrating the economic viability of a high-speed aircraft fleet [1-4]. These concepts make use of unexploited flight routes in the stratosphere, offering a solution to the presently congested flight paths while ensuring a minimum environmental impact in terms of emitted noise and green-house gasses, particularly during the stratospheric cruise phase. Only a dedicated multi-disciplinary and highly integrated design concept could realize this, where aero-thermodynamic issues are evaluated together with the structural and propulsive issues, in the frame of a highly multidisciplinary project [5-8].

In this context, the STRATOFLY (Stratospheric Flying Opportunities for High Speed Propulsion Concepts) project has been funded by the European Commission, under the framework of Horizon 2020 plan with the main objective of shortening the flight time of one order of magnitude with respect to the state of the art of civil aviation, for civil passenger flights of at least 300 passengers along long haul and antipodal routes [9-13].

This paper describes the thermal design processes of some vehicle cooling system showing either the methodology and the supporting numerical simulations. In particular, it focuses on two different regions that are both subjected, for different reasons, to severe overheating: air-intake leading edges and the combustion chamber. Indeed, the first are subjected to convective over-heating due to their very small radii (about 2 mm), while the second is basically the propulsive flow path. Therefore ad-hoc efficient cooling systems must be designed.

Present work shows the methodology, the numerical simulation and the main results for the two cooling systems.

2. Air-Intake leading edge cooling system design [14]

STRATOFLY MR3 is a highly integrated vehicle, where propulsion, aerothermodynamics, structures and on-board subsystems are strictly interrelated to one another, as highlighted in Figure 1 [4;5;6].

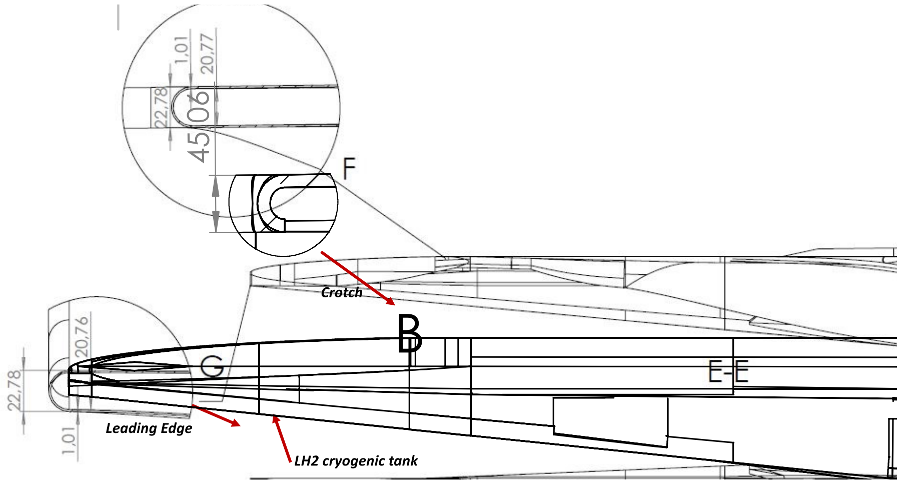

Figure 1. STRATOFLY MR3 arrangement constraints within the air intake leading edges

Air-intake leading edges are subjected to convective over-heating due to their very small radii (about 2 mm). Therefore, ad-hoc efficient cooling systems must be designed. Heat pipes systems have been chosen as driving system. First of all, design and sizing activities consist in the definition of feasible integrated architectures, and selection of the most appropriate working fluids and compatible wick and case materials. The analysis of the heat transfer limits (the capillary, entrainment, viscosity, chocking and boiling limits) is here suggested as guideline for the identification of a suitable design space and rational down-selection of the most promising solution. Different alternative solutions have been thoroughly analysed, including two different heat pipes layouts (single tubular and dual-channel architecture), five liquid metals as fluids (Mercury, Caesium, Potassium, Sodium and Lithium) and relative wick and case materials (Steel, Titanium, Nickel, Inconel® and Tungsten) and three leading-edges materials (CMC, Tungsten with low emissivity painting and Tungsten with high emissivity painting). Considering the volumetric constraints imposed by the peculiar design of the embedded air-intake of the MR3, a dedicated heat-pipe architecture, inspired by the NASP project, has been developed. This architecture has been suggested for both the lower lip as well as for the crotch air-intakes. In both cases, the proximity of the foremost cryogenic tanks suggests a longitudinal orientation of the pipes, parallel to the longitudinal axis of the vehicle. The 22 mm radius of the air-intake leading edges allows to adopt a dual-channel architecture instead of a more traditional tubular architecture. The proposed solution increases the exposed area of the evaporator, thus potentially increasing the heat transfer capability. As schematically reported in Figure 2, the suggested heat pipe solution is completely integrated into the air-intake structure, assuming that the heat pipe case is perfectly bonded with the panels of the aircraft skin. Eventually, a perfect bonding is also ensured between the case and the wick. Finally, it is worth noting that the rearrest part of the condenser region shall be properly interfaced with the tank external structure, to guarantee the required heat rejection.

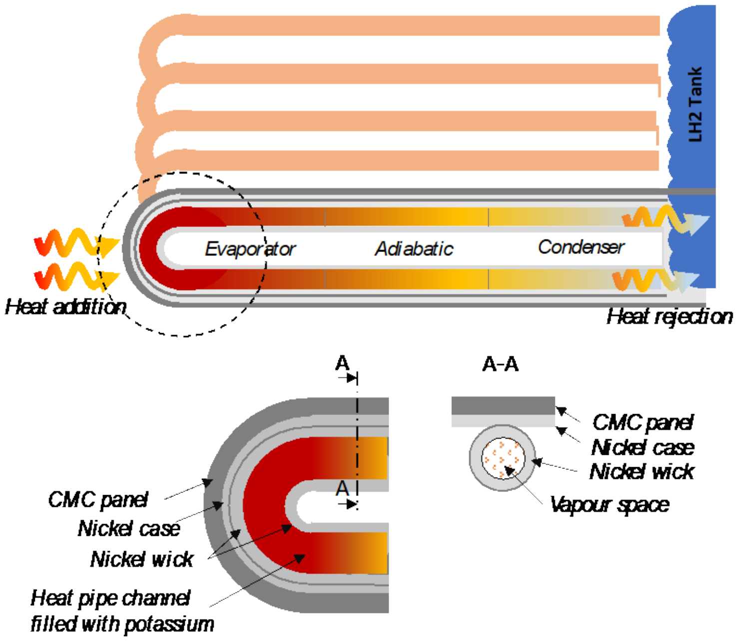

Figure 2. Overall heat pipe arrangement for the selected case study

2.1 Numerical Simulations

Several finite element models have been developed to perform a parametric study aimed, on the one hand, at evaluating the pipe performance and, on the other hand, at optimizing the air intake layout in terms of material and geometric thicknesses. A mesh convergence analysis led to a finite element model of about 5000 nodes and 1000 HEXA solid elements with an average element quality of 0.95.

Three different leading edges materials have been considered and analysed: *Tungsten; tungsten coated by high emissivity paint (ε=0.9); full CMC.* Finally, the latter has been chosen as the best material. Indeed, different simulations have been performed varying the subtractive heat fluxes from the pipe. This allows checking the effect on maximum temperature on the crotch. Figure 3 shows the different fluxes whose peaks range from 700 kW/m2 for run 1 to about 950 kW/m^2 for run 4. Figure 3 shows also the corresponding results in terms of maximum temperature on the crotch. It is clear that CMC acts as a very effective thermal barrier. Indeed, an increment in subtractive heat fluxes of the 25%, results in a 4.85% temperature reduction. Finally, run 4 conditions are retained because this scenario keeps the CMC temperature under the theorical service operative temperature fixed at 1600°C. Figure 4 shows the thermal map on CMC leading edge at maximum time instant. The temperature reaches, in this case, a peak value of 1598°C at 2634s. Figure 4 shows also the thermal behaviour of the CMC panels.

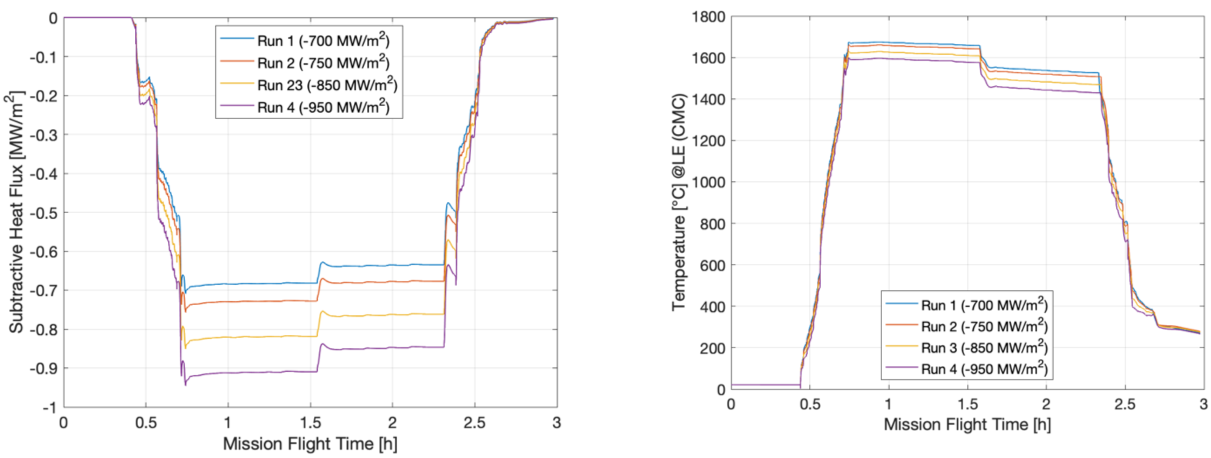

Figure 3. (a) Subtractive heat fluxes from heat pipe; (b)Maximum temperature evolution at CMC crotch w.r.t different subtractive heat fluxes

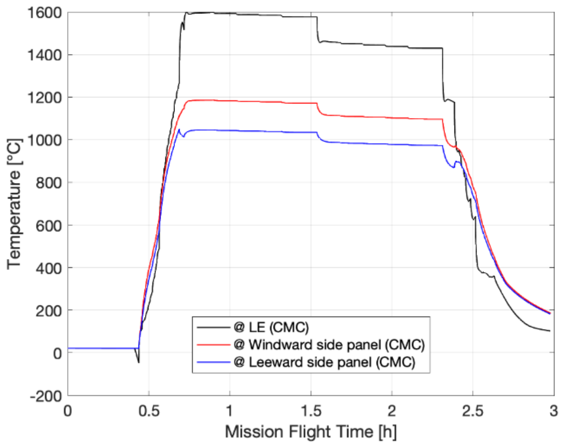

Figure 4. (a) Maximum temperature evolution at CMC crotch and at CMC leeward side and windward side panel

A numerical APDL code has been set-up to verify the effective subtractive heat flux guaranteed by the selected heat pipe arrangement. The numerical code simulates the convection phenomenon as an equivalent conduction through pipe structure, where the thermal conductivity of the overall heat pipe is calculated by Eq. (1):

$$K_{eff} = \frac{Q * L_{eff}}{A_{hp} * (T_{evaporator} - T_{condenser})} \qquad \text{Eq. (1)}$$

When the heat pipe is active, its thermal conductivity typically ranges from 10,000 to 100,000 W/m K, that is 250 to 500 times the thermal conductivity of solid copper and aluminium, respectively. Figure 17 shows the flowchart of APDL code.

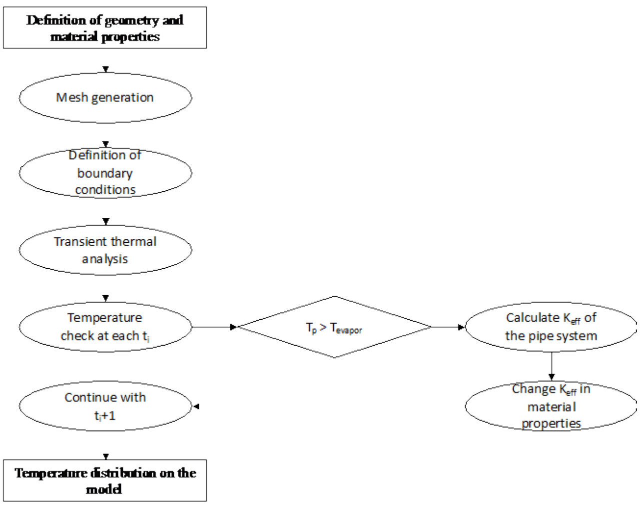

Figure 5. Flow Chart- Simulation Process

During the analysis the code retrieves the heat flux value (Q) at the interface Heat Pipe-Internal Crotch, the temperature in the evaporator and condenser zone ($T_{evaporator}, T_{condenser}$) at every simulation step. A check on the temperature in evaporator zone at each step is performed and if $T_{evaporator}$ is higher than the boiling temperature of Potassium, K_{eff} can be estimated using Eq. (1), using the $T_{condenser}$ and Q associated to the current step. Once the K_{eff} is evaluated, the conductivity of each material is updated accordingly.

Finally, the value of the effective subtractive heat flux derived by Pipe activation (0.72 MW/m^2) is in line with the most conservative value (0.7 MW/m^2) hypothesized during the thermal design step (the so-called run 1 in Figure 3) (Figure 6).

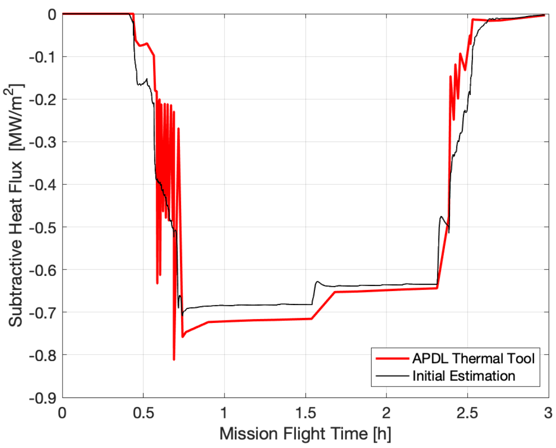

Figure 6. Comparison of Subtractive Heat Flux estimation via APDL with reference to the initial guess

2.2 Results

FEM analysis suggest the adoption of a Nickel-Potassium liquid metal heat pipe completely integrated in a platelet air-intake leading edge made of CMC material.

3. Combustion chamber cooling system design

A convective heat flux distribution is imported on combustion chamber surfaces to simulate the dual-mode-ramjet (DMR) engine operation during the flight (see Figure 7). The distribution considers the presence of a cooling jacket on the combustor section, i.e. the convection applied is a net convection between the hot contribution coming from CFD calculation (see Figure 8), i.e. the effect of air-hydrogen combustion process, and the subtractive contribution of the cooling jacket.

In order to correctly estimate the cooling jacket subtractive heat fluxes, input data from POLITO EcoSimpro TEMS have been acquired in terms of pressure, temperature and mass flow along the whole trajectory (Figure 8; Figure 9), also with respect to the previous LAPCAT MR2.4 (Table 1);. Fixing two relevant conditions at Mach 8 and Mach 6 ascent, and considering the impacted surface area of 39.45 m^2 (Figure 11) it is possible to compute the cooling jacket subtractive heat flux of about 1.5 MW/m^2 for Mach 8 (Table 2) and of about 1.75 MW/m^2 at Mach 6 (Table 3) with the following formulation (Eq.2):

$$H_f = \frac{\dot{m}c_p(T_{outlet} - T_{inlet})}{Area} \qquad \text{(Eq. 2)}$$

Moreover, other boundary conditions have been considered.

In particular, a radiation to very conservative hot ambient temperature condition (as indicated in Figure 13) where the air estimated temperature profile along the trajectory is depicted) with emissivity value of ε=0.8 is set up for internal surfaces of combustion chamber, nozzle and divergent section. (see Figure 12).

To properly integrate the cooling effect coming from LH2 tanks within thermal analysis all along the reference mission, a simple analysis of LH2 tanks reference temperatures has been done by PoliTo and results, summarized in (Figure 14), show how estimated temperature varies from 20 K to 80 K for internal surfaces and from 200 K to 260 K for external ones. These values have been considered as boundary conditions for thermal analysis.

Finally, a radiation surface to surface condition between the combustion chamber and the leeside panel has been imposed with emissivity value of 0.8. (Figure 15)

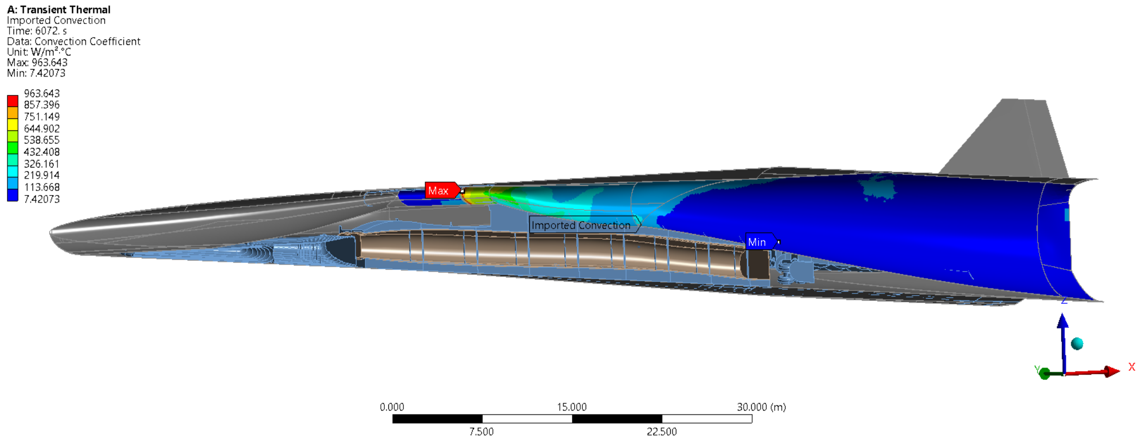

Figure 7. Imported convection on internal combustion chamber and nozzle surfaces.

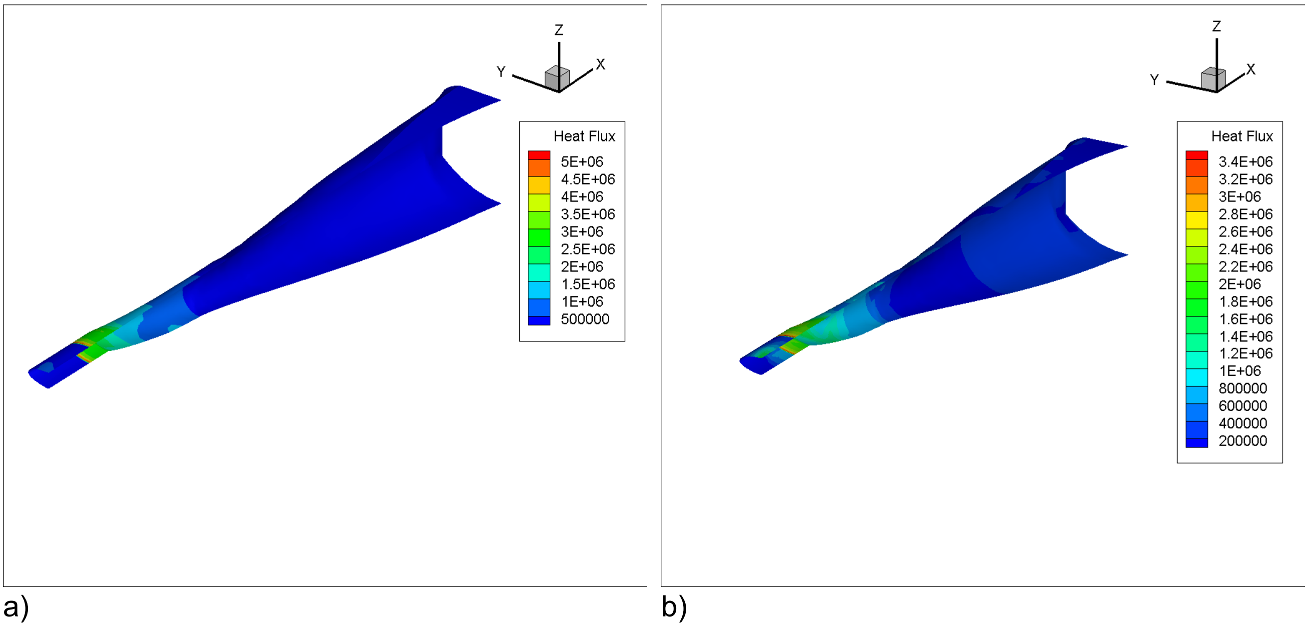

Figure 8. Heat flux in combustion chamber and nozzle computed at Mach 6 (a) and Mach 8 (b).

Component – Side	**Pressure [Pa]**		**Temperature [K]**	
	STRATOFLY MR3	**LAPCAT MR2.4**	**STRATOFLY MR3**	**LAPCAT MR2.4**
Pump – Inlet	1e5	1e5	20	20
Pump – Outlet	71.2e5	80e5	80	27
Cooling Jacket – Inlet	71.2e5	80e5	180	27
Cooling Jacket - Outlet	71e5	79.7e5	566	686

Table 1. TEMS Parameters comparison at Mach 8 (EcosimPro).

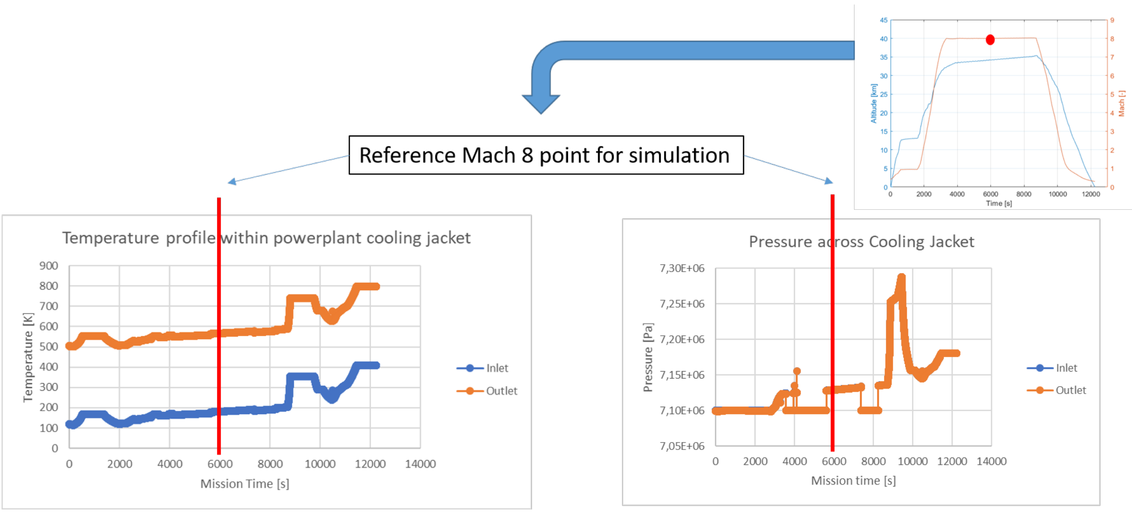

Figure 9. Temperature (left) and pressure (right) profiles within cooling jacket along the trajectory.

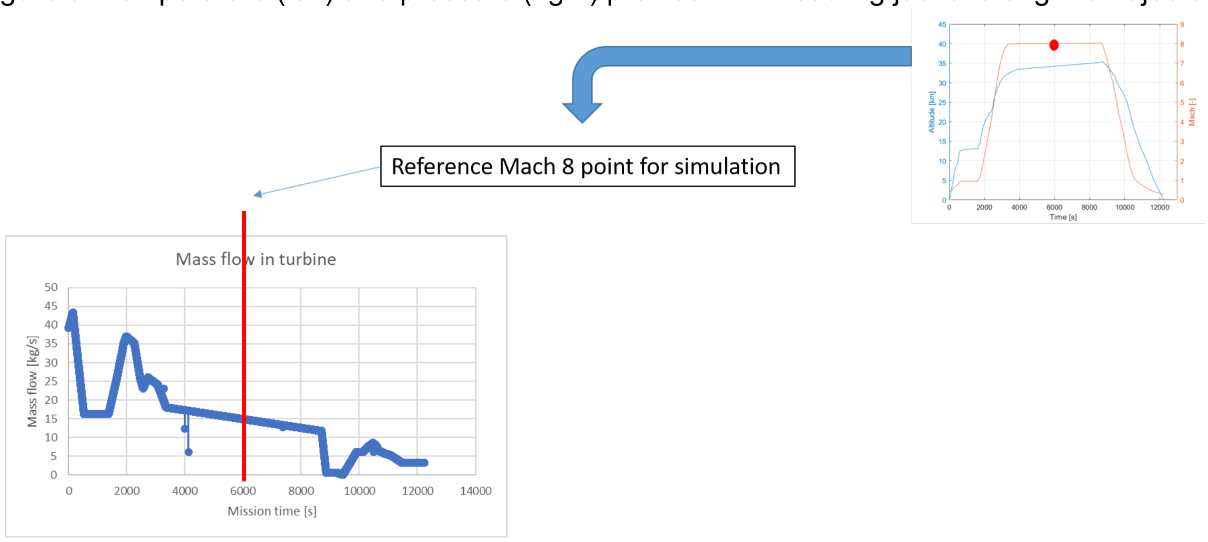

Figure 10 Mass flow in turbine along the trajectory.

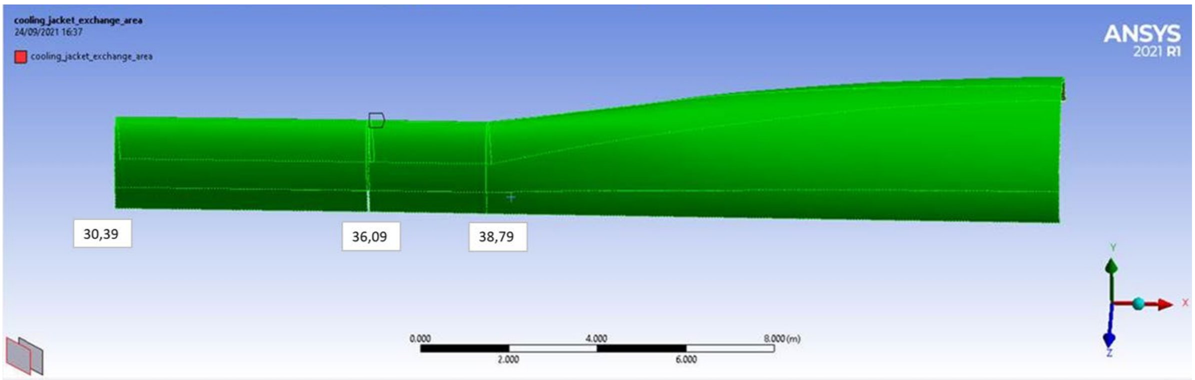

Figure 11. Cooling jacket section area.

Data		Unit	Source
Cp (H2 gaseous)	14200.00	J/kg/K	NIST
Lateral Surface	39.45	m^2	L=8m combustor+2D nozzle
H2 mass flow rate	10.78	kg/s	as injected at struts
outlet temperature	566.00	K	cooling jacket L=8m
inlet temperature	180.00	K	cooling jacket L=8m
Heat flux	**1497777.85**	**W/m^2**	

Table 2. Cooling jacket subtractive heat flux at Mach 8.

Data		Unit	Source
Cp (H2 gaseous)	14200.00	J/kg/K	NIST
Lateral Surface	39.45	m^2	L=8m combustor+2D nozzle
H2 mass flow rate	12.64	kg/s	as injected at struts
outlet temperature	566.00	K	cooling jacket L=8m
inlet temperature	180.00	K	cooling jacket L=8m
Heat flux	**1756207.05**	**W/m^2**	

Table 3. Cooling jacket subtractive heat flux at Mach 6.

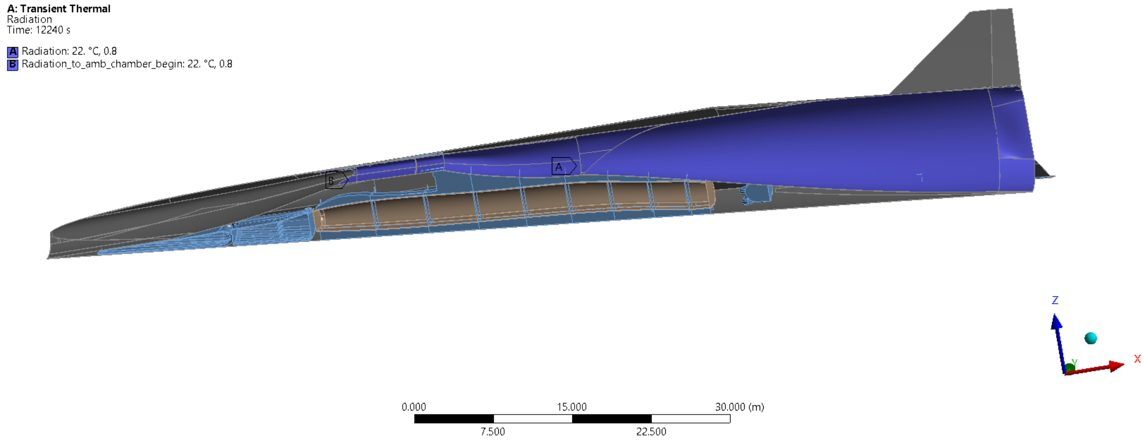

Figure 12. Radiation to ambient of Engine surfaces.

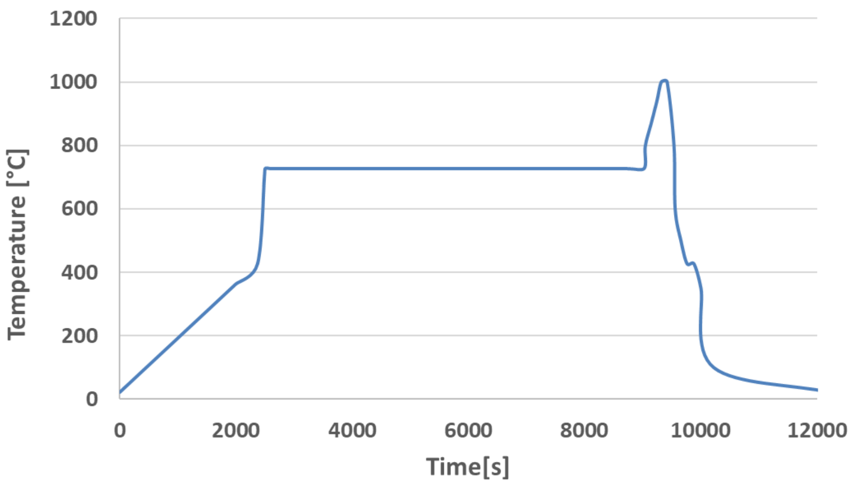

Figure 13. Ambient Temperature evolution in combustion chamber along the trajectory.

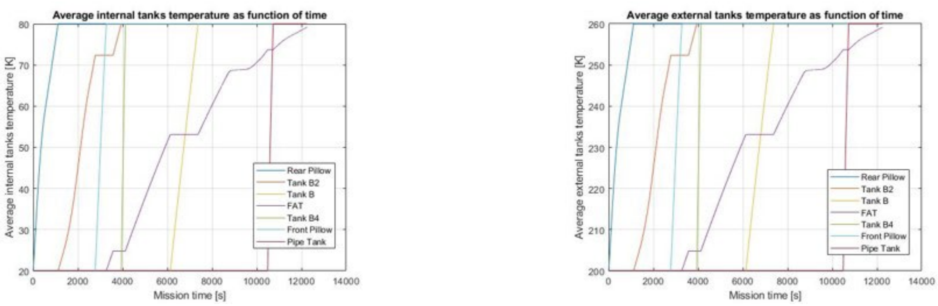

Figure 14. Average internal and external tanks temperature as function of time.

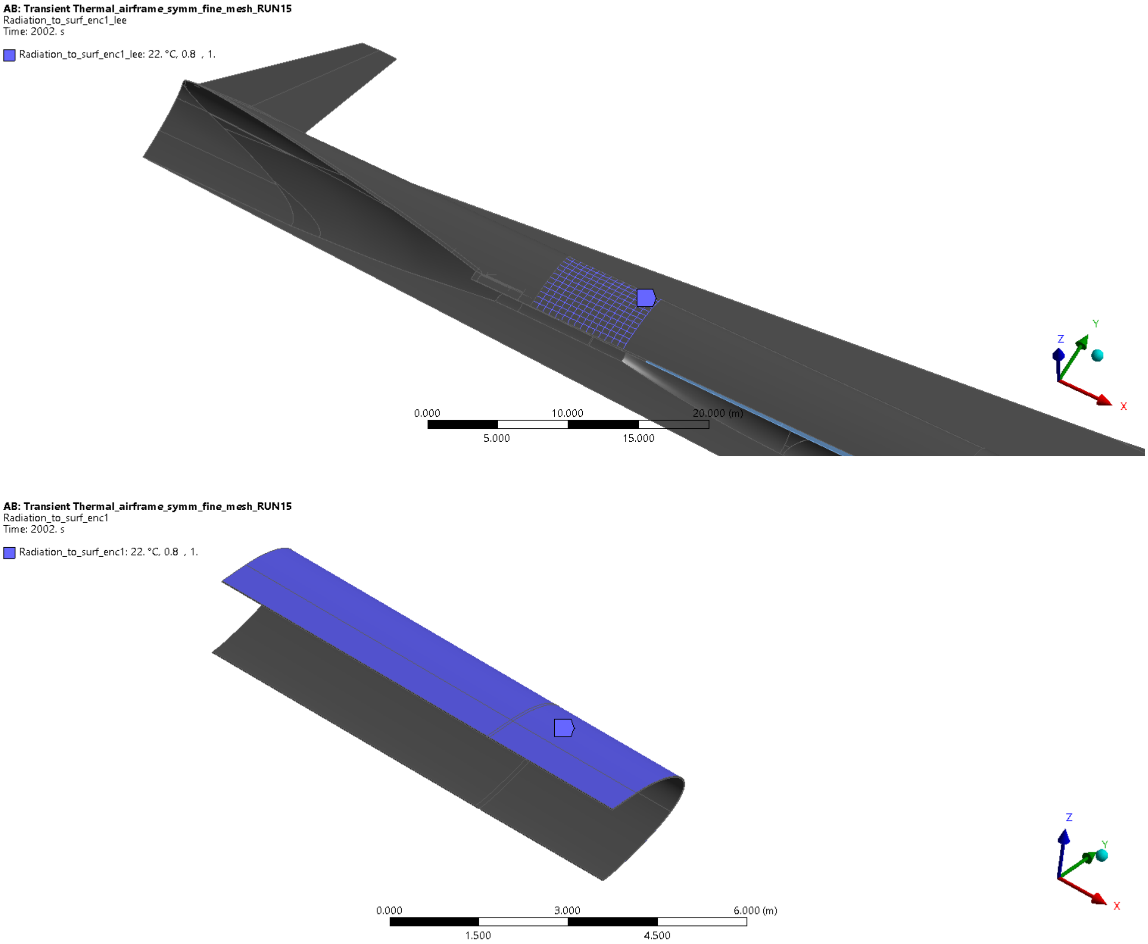

Figure 15 Radiation surface to surface between combustor and leeside panel.

3.1 Main results

Figure 16 and Figure 17 show the temperature map at maximum temperature time instant on the propulsive flow path respectively at Mach 8 and Mach 6 flight conditions. The following aspects must be highlighted:

- The effect of the radiation surface to surface between the external faces of combustor and the airframe leeside panels is effective to lower the temperature under CMC allowable. Nevertheless, due to the low CMC conductivity (the CMC acts as thermal barrier) the internal surfaces do not beneficiate of this condition.
- The heat sink effect of front additional tank is evident along the path. Nevertheless, the beneficial effect is localized to the perfect contact areas.
- At Mach 8 the combustor exceeds the indicated allowable of about 300 °C, but at Mach 6 the overcome is of about 900°C. This is linked to an excessive heat load. Indeed, as shown in Figure 8 that area is impacted by extremely high heat fluxes values for a very long time (about 500 s at Mach 6, and about 6030 s at Mach 8) leading to an enormous Heat Load (about 1500 MW at Mach 6 and 1000 MW at Mach 8).

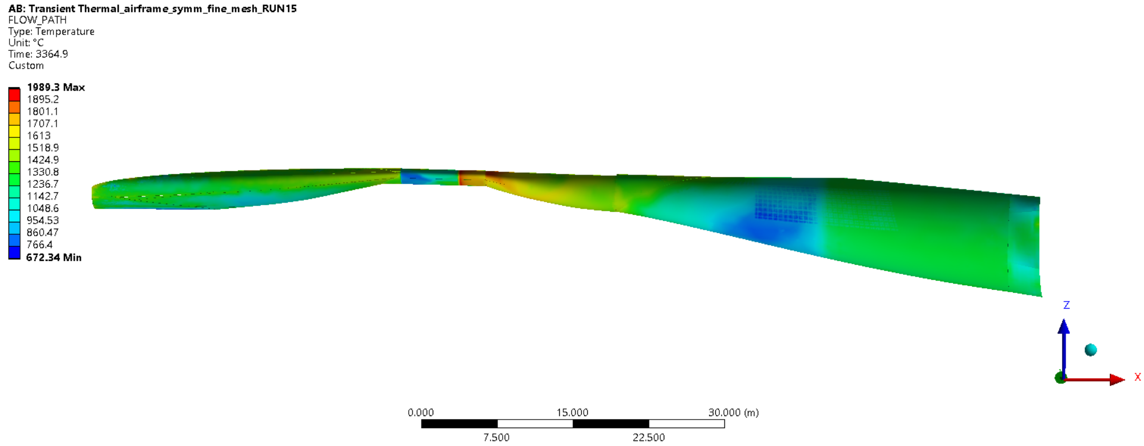

Figure 16 Temperature map at maximum time instant on the propulsive flow path (Mach 8).

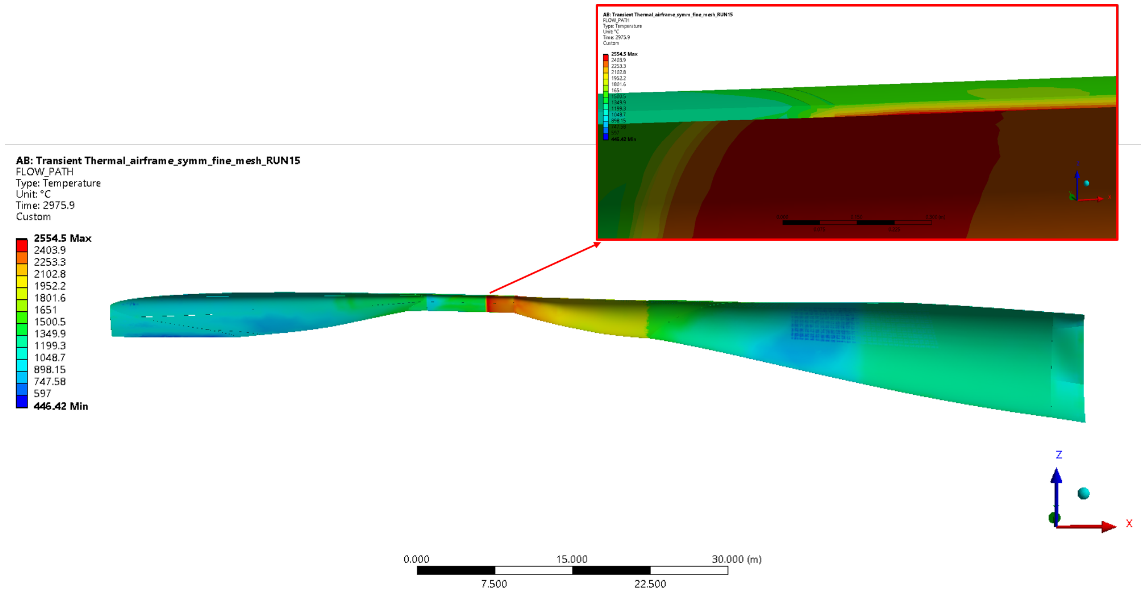

Figure 17 Temperature map at maximum time instant on the propulsive flow path (Mach 6).

4. General conclusions

FEM numerical results stressing on the solutions that provide thermal integrity of the vehicle are presented.

Main results can be summarized as follows:

a. **The CMC airframe structure is thermally safe** (temperature always under 1600°C).

b. The heat pipes designed and presented in the second section are confirmed to be effective in cooling the crotch

c. The combustor exceeds the CMC temperature allowable at Mach 6 and Mach 8. This is linked to an excessive heat load. Therefore, further detailed CFD computations as well as detailed thermo-structural FEM analysis must be set to ensure the combustor survival along the proposed trajectory, by considering a larger subtractive heat flux (i.e. a more effective cooling jacket for the combustor) if TEMS is able to satisfy this new requirement, and/or a more performant CMC material for combustor section.

5. Contact Author Email Address

For contact please mail to: r.scigliano@cira.it

6. Copyright Statement

References

[1] Steelant J., Varvill R., Defoort S., Hannemann K., Marini M. Achievements Obtained for Sustained Hypersonic Flight within the LAPCAT-II Project. *20th AIAA International Space Planes and Hypersonic Systems and Technologies Conference*, Glasgow, Scotland, AIAA-2015-3677, 6-9 July 2015.

[2] Steelant J. ATLLAS: Aero-thermal loaded material investigations for high-speed vehicles. *15th AIAA International Space Planes and Hypersonic Systems and Technologies Conference*. Dayton, Ohio, USA, AIAA 2008-2582, doi 10.2514/6.2008-2582, 28 April – 1 May 2008.

[3] Steelant J. et al. Conceptual Design of the High-Speed Propelled Experimental Flight Test Vehicle HEXAFLY, *20th AIAA International Space Planes and Hypersonic Systems and Technologies Conference.* Glasgow, Scotland, AIAA 2015-3539, 6-9 July 2015.

[4] Di Benedetto S. et al. Multidisciplinary Design and Flight Test of the HEXAFLY-INT Experimental Flight Vehicle Hexafly-Int. *HiSST: International Conference on High-Speed Vehicle Science Technology*. Moscow, Russia, 2018

[5] Scigliano R., Marini M., Fusaro R., Viola N. Preliminary Aero-Thermal Assessment of the High-Speed Propelled Vehicle STRATOFLY, *32nd ISTS (International Symposium on Space Technology and Science) & 9th NSAT (Nano-Satellite Symposium).* Fukui, Japan, 2019-e-06, June 2019.

[6]. Scigliano R., Marini M., P. Roncioni, Fusaro R., Viola N., STRATOFLY High-Speed Propelled Vehicle Preliminary Aero-Thermal Design. *International Conference on Flight Vehicles, Aerothermodynamics and Re-Entry Missions and Engineering FAR 2019.* Monopoli, Italy, 30th September - 3rd October 2019.

[7] Scigliano R., De Simone V., Marini M., P. Roncioni, Fusaro R., Viola N. Preliminary Finite Element Thermal Analysis of STRATOFLY Hypersonic Vehicle*. 23rd AIAA International Space Planes and Hypersonic*

Systems and Technologies Conference - AIAA HYPERSONICS 2020. Montreal, Quebec, Canada, 10.2514/6.2020-2422, March 10-12, 2020.

[8] Scigliano R., De Simone V., Marini M., Fusaro R., Ferretto D., Viola N., Thermal Protection System Preliminary Design of STRATOFLY High-Speed Propelled Vehicle, *32nd Congress of the International Council of the Aeronautical Sciences*. Shanghai, China, ICAS2020-0493, 6-10 September 2021.

[9] Viola N., Fusaro R., Ferretto D., Gori O., Saracoglu B., Ispir A.C., Schram C., Grewe V., Plezer J.F., Martinez J., Marini M., Cutrone L., Saccone G., Hernandez S., Lammers K., Vincent A., Hauglustaine D., Liebhardt B., Linke F., Bodmer D., Nilsson T., Fureby C., Ibron C. H2020 STRATOFLY PROJECT: FROM EUROPE TO AUSTRALIA IN LESS THAN 3 HOURS (2021) *Proceedings of 32nd Congress of the International Council of the Aeronautical Sciences*, ICAS 2021.

[10] Viola N., Fusaro R., Gori O., Marini M., Roncioni P., Saccone G., Saracoglu B., Ispir A.C., Fureby C., Nilsson T., Ibron C., Zettervall N., Bates K.N., Vincent A., Martinez-Schram J., Grewe V., Pletzer J., Hauglustaine D., Linke F., Bodmer D. Stratofly MR3 – how to reduce the environmental impact of high-speed transportation (2021) *Proceedings of AIAA Scitech 2021* Forum, pp. 1 - 21,

[11] Viola, N., Fusaro, R., Saracoglu, B. et al. Main Challenges and Goals of the H2020 STRATOFLY Project. *Aerotec. Missili Spaz.* 100, 95–110 (2021). https://doi.org/10.1007/s42496-021-00082-6

[12] Viola N., Fusaro R., Vercella V. Technology roadmapping methodology for future hypersonic transportation systems (2022) *Acta Astronautica*, 195, pp. 430 - 444, DOI: 10.1016/j.actaastro.2022.03.038

[13] Viola N., Roncioni P., Gori O., Fusaro R. Aerodynamic characterization of hypersonic transportation systems and its impact on mission analysis (2021) *Energies*, 14 (12), art. no. 3580, DOI: 10.3390/en14123580

[14] Fusaro R., Ferretto D., Viola N., Scigliano R., De Simone V., Marini M., Liquid Metals Heat-Pipe solution for hypersonic air-intake leading edge: Conceptual design, numerical analysis and verification, *Acta Astronautica* (2022), doi: https://doi.org/10.1016/j.actaastro.2022.05.034.